Article

Measurements of J/ψ Production vs. Event Multiplicity in Forward Rapidity in $p + p$ Collisions in the PHENIX Experiment

Zhaozhong Shi

Special Issue

Zimányi School – Heavy Ion Physics

Edited by
Prof. Dr. Máté Csanád, Dr. Péter Kovács, Dr. Sándor Lökös and Dr. Dániel Kincses

Article

Measurements of J/ψ Production vs. Event Multiplicity in Forward Rapidity in $p + p$ Collisions in the PHENIX Experiment

Zhaozhong Shi [†][ORCID] on behalf of the PHENIX Collaboration

Physics Division, Los Alamos National Laboratory, Los Alamos, NM 87545, USA; zhaozhongshi@lanl.gov;
Tel.: +1-415-350-3181
† Current address: Physics Department, Brookhaven National Laboratory, Upton, NY 11973, USA.

Abstract: J/ψ, a charmonium bound state made of a charm and an anti-charm quark, was discovered in the 1970s and confirmed the quark model. Because the mass of charm quarks is significantly above the quantum chromodynamics (QCD) scale Λ_{QCD}, charmonia are considered excellent probes to test perturbative quantum chromodynamics (pQCD) calculations. In recent decades, they have been studied extensively at different high-energy colliders. However, their production mechanisms, which involve multiple scales, are still not very well understood. Recently, in high-multiplicity $p + p$ collisions at RHIC and at the LHC, a significant enhancement of J/ψ production yield has been observed, which suggests a strong contribution of multi-parton interaction (MPI). This is different from the traditional pQCD picture, where charm quark pairs are produced from a single hard scattering between partons in $p + p$ collisions. In this work, we will report the J/ψ normalized production yield as a function of normalized charged particle multiplicity over a board range of rapidity and event multiplicity in the $J/\psi \to \mu^+\mu^-$ channel with PHENIX Run 15 $p + p$ data at $\sqrt{s} = 200$ GeV. The results are compared with PYTHIA 8 simulations with the MPI option turned on and off. Finally, the outlooks of J/ψ in $p + Au$ and $Au + p$ collisions, along with color glass condensate (CGC) predictions and the multiplicity-dependent $\psi(2S)/J/\psi$ ratio in $p + p$ data, will be briefly discussed.

Keywords: quantum chromodynamics; charmonium; multi-parton interactions; production yield; high event multiplicity; $p + p$ collisions; initial state effect; final state interaction; hadronization; color glass condensate

1. Introduction

In 1974, J/ψ, a charmonium-bound state made of charm and anti-charm quark ($c\bar{c}$) was discovered at Brookhaven National Laboratory [1] and the Stanford National Linear Accelerator [2] and confirmed the existence of charm quarks [3] and validated the quark model. Because the charm quark mass is above the QCD scale Λ_{QCD}, the production of a $c\bar{c}$ pair in high-energy collisions is perturbative, which makes J/ψ an excellent probe to test pQCD calculations.

The production of J/ψ at high-energy hadronic colliders involves multiple stages across many different scales. In recent decades, J/ψ has been studied extensively at different colliders [4–6]. Nonetheless, the description of J/ψ production is still not fully developed and cannot reach very high precision. However, thanks to the QCD factorization theorem [7], hard processes, which are perturbatively calculable, are factorized from soft processes, which are non-perturbative but can be modeled phenomenologically and constrained by experiments. This allows us to apply pQCD to calculate the production cross-section of J/ψ. We can test QCD at high-energy colliders through a comparison of the J/ψ production data with model calculations.

In hadronic collision events, both elastic and inelastic scatterings may occur. Experimentally, we are interested in inelastic collision events. There are two types of inelastic hadronic collision events: diffractive and non-diffractive dissociations [8]. In this work, we focus on J/ψ, produced in non-diffractive hadronic collision events, which can be denoted as $pp \to J/\psi + X$.

A simple sketch of J/ψ production in high-energy hadronic collision events can be summarized as below:

Initial Dynamics of Partons: According to the Parton Model, the structure of hadrons can be described by constituent partons [9]. The initial dynamics of partons are non-perturbative but can be parametrized by parton distribution function (PDF) [10]. They can be measured in deep inelastic scattering experiments at different colliders and related with each other via scaling [7]. Alternatively, phenomenological approaches [11], such as String Percolation [12] and Color Glass Condensate [13], can be applied to model the incoming hadrons. These models have been compared with experimental data such as charged particle p_T spectra and rapidity distribution $dN_{ch}/d\eta$ and demonstrate reasonably good agreement [14,15].

Initial State Interactions: They occur among energetic partons before hard scatterings. One example is the soft radiation of partons [16], which is called the initial state radiation (ISR). ISR will influence the initial heavy-quark pair production [17]. Usually, the effect can widen $c\bar{c}$ azimuthal angle correlation [18] and broaden the p_T spectra [19].

Hard Partonic Scattering: Energetic partons scatter off each other with large momentum transfers. In the traditional pQCD picture, it is simply described as a single hard scattering between two partons in each collision. They can be calculated analytically by pQCD with Feynman diagrams to a very high precision [20]. At RHIC, the $c\bar{c}$ pair production is dominated by gluon–gluon fusion: $gg \to c\bar{c}$.

Multiple Parton Interaction (MPI): MPI is an elaborate paradigm to describe the partonic interaction stage at high-energy colliders at RHIC, Tevatron, and the LHC [21]. According to MPI, one hard scattering, accompanied by several semi-hard interactions, takes place in each collision. All of them need to be included in the partonic scattering amplitudes. At present, high-energy hadronic colliders create more phase space for MPI to occur. Many studies at the LHC suggest MPI should be included to better describe the data [22].

Hadronization: In the final state, the $c\bar{c}$ pairs will lose energy via radiation and evolve into the color-neutral J/ψ bound state. Because this process is also soft and non-perturbative, many phenomenological models have been developed to describe the $c\bar{c} \to J/\psi$ process in different collision systems. Selected examples of theoretical models are listed below:

Non-Relativistic QCD (NRQCD): This is an effective field theory approach to describe the hadronization of $c\bar{c}$ pairs thanks to their large mass compared to its internal kinetic energy, which results in a slow speed β [23] within the non-relativistic limit $\beta << 1$. NRQCD includes perturbative short-distance and non-perturbative long-distance effects for a range of strong coupling α_s. To the leading order (LO), there are two mechanisms describing charmonium production.

- Color Singlet (CS): The $c\bar{c}$ pairs are in the color-singlet state with the same quantum number as the $c\bar{c}$ bound state in J/ψ. When the $c\bar{c}$ pair kinematics reach the J/ψ mass, they will bind together [24].
- Color Octet (CO): The $c\bar{c}$ pairs are in the color-octet state carrying net color changes and emit extra gluons [25] to reach the color-neutral state, which results in additional hadron production associated with the J/ψ observed in the J/ψ-hadron correlation studies [26].

NRQCD predicts sizable transverse polarization of J/ψ, which has also been observed experimentally [27]. There are other phenomenological models, such as the Color Evaporation Model [28], Statistical Hadronization Model [29], and Color String Reconnection

Model [30], that describe the J/ψ hadronization. Currently, physicists are testing all these models with experimental data.

Final State Interaction (FSI): In the final state, the newly formed J/ψ mesons may still interact with comoving particles nearby [31]. In the elastic scenario, J/ψ kinematics will be modified. Inelastically, J/ψ may possibly be broken up [32]. Hence, the final state comover effect may affect J/ψ production yield and will become more prominent at high levels of multiplicity. Experimentally, the final state comover effect can be studied by J/ψ-hadron femtoscopic correlation measurements [32]. Theoretically, FSI has also been implemented in the EPOS event generator [33].

Experimental Observables: All the above-mentioned processes will contribute to the final production of J/ψ, which can be reconstructed from its decay particles with detectors in the experiment. The experimental observables used to study J/ψ production may be the production yield as a function of event activity for fully reconstructed J/ψ. Experimentally, the event activity is quantified by charged particle multiplicity. The production yield, as a function of event multiplicity, can probe the processes at the partonic level and will shed light on the interplay between soft and hard particle production [34].

In particular, we can use a relative quantity: the normalized J/ψ yield $R \equiv N^{J/\psi}/\langle N^{J/\psi} \rangle$ as a function of normalized charged particle multiplicity $N_{ch}/\langle N_{ch} \rangle$. In experiments, this observable has an advantage because it can cancel the luminosity and some efficiency corrections, such as J/ψ acceptance and reconstruction efficiency, which ultimately reduces the systematic uncertainties. Theoretically, in the string percolation picture [12], there is a simple scaling of $N^{J/\psi}$ by the number of color strings N_s at the partonic level, which is similar to N_{coll} in heavy-ion collisions at the nucleon level. Moreover, N_{ch} is scaled by N_s, another analog to the N_{part} scaling for soft particle production in heavy-ion collisions. Therefore, this is also inspired by theoretical perspectives. The normalized J/ψ yield as a function of normalized charged particle multiplicity measurements was studied by experiments conducted at RHIC and the LHC over different kinematic regions.

Autocorrelation: The J/ψ itself can contribute to the charged particle multiplicity in many different ways, as listed below [35]:

- The J/ψ decay daughters, such as the dipion, dielectron, and dimuon pairs.
- The extra gluons emitted from the $c\bar{c}$ pair in the color-octet state producing additional charged hadrons [26].
- The J/ψ cluster collapsing into hadrons [36].
- The feed down from b-hadron decays for non-prompt J/ψ.

Generally speaking, the autocorrelation increases N_{ch} in J/ψ events compared to minimum bias (MB) events. Reducing the autocorrelation effects can improve our study for dedicated physics processes.

2. Recent Developments

Today, with the advancement of technologies related to detector instrumentation, high-performance computing, and artificial intelligence, we are moving toward a high-precision QCD era. Many novel studies of J/ψ production have been conducted at RHIC and the LHC.

Recently, the ALICE Collaboration reported results on J/ψ production measured in dielectron channel with the LHC Run 2 pp data at $\sqrt{s} = 5, 7, 13$ TeV [37–39]. The measurements of the J/ψ-normalized yield are performed in both middle- and forward-rapidity regions over a wide range of normalized charged particle multiplicities [40]. The normalized J/ψ yield, as a function of $N^{J/\psi}/\langle N^{J/\psi} \rangle$ at mid-rapidity, generally lies above the forward-rapidity region. A significant enhancement of J/ψ production with respect to linear scaling is observed at high multiplicities for both middle and forward rapidities [39]. Several theoretical models incorporating both initial state effects and MPI attempt to explain the data [39].

At RHIC, the STAR experiment carried out the J/ψ studies in the dielectron channel, which only shows up to about three units of average charged particle multiplicities at a

rapidity of $|y| < 1$ [41]. The data are presented in different p_T regions. However, the results also suggest a slight enhancement for J/ψ production and are comparable to ALICE at the LHC energy rate. The increase becomes steeper at a higher p_T and multiplicity region, although this difference is not significant due to the large uncertainties and does not occur at a very high event multiplicity, where the FSI is reduced and MPI effect is more prominent. The STAR result are generally well described by CEM, CGC, and NLO with NRQCD calculations at different p_T regions. However, no conclusion regarding the use of MPI for J/ψ production at RHIC at mid-rapidity and near the average charged particle multiplicity has been drawn.

Phenomenologically, the MPI effect plays a significant role in charm-quark production [42]. In the MPI picture, the average number of heavy-quark pairs in pp collision increases compared to the traditional pQCD picture of single hard scattering [43]. Along with the color reconnection model for J/ψ hadronization treatment, a significant enhancement of the J/ψ production cross-section [30] is predicted. Hence, the linear scaling assumed in the traditional pQCD picture does not hold [44].

From the simulation side, the latest versions of PYTHIA 8 event generator incorporated many physics processes, including ISR, hadronization, and FSR, in addition to MPI, to describe underlying events in high-energy pp collisions [45]. PYTHIA 8 simulations are able to reproduce the charged particle p_T spectra and $dN/d\eta$ with reasonably good agreement at RHIC with Detroit tune [46] and the LHC with Monash tune [47]. PYTHIA users can turn MPI on and off, use different underlying event tunes, and adjust the CSM and COM contribution in $c\bar{c} \rightarrow J/\psi$ to compare with the data.

The J/ψ produced from the recombination of the $c\bar{c}$ pair described in the Introduction is traditionally considered the dominant production mechanism of J/ψ [48] and will lead to a substantial amount of transverse polarization. However, recently, at the LHC, unpolarized J/ψ production from jets, an alternative production mechanism in pp [49] and PbPb [50] collisions was observed by the CMS experiment. Moreover, LHCb has shown that unpolarized J/ψ, down to low p_T, is produced from jet fragmentation in pp collisions [51]. J/ψ are observed to be hadrons within the jet cones' radius. The J/ψ produced from jets will have different production processes compared to those described above.

Most J/ψ measurements are carried out in non-diffractive dissociation events at hadronic colliders. There are also some theoretical efforts to study novel QCD with J/ψ production in single diffractive pp collisions via Pomerons exchange ($pp \rightarrow pX$) [52]. Measurements on a single diffractive pp cross-section have also been carried out by the ALICE [53] and ATLAS experiments [54] at the LHC.

These latest developments motivate us to investigate J/ψ at high event multiplicities in forward-rapidity at RHIC. The PHENIX detector is capable of carrying out this physics [55]. Thanks to the excellent tracking, vertexing, and muon performance of the PHENIX detector, we can perform charmonium studies in the forward-region up to high multiplicities. Historically, the research on the event multiplicity dependence of J/ψ production in small systems with PHENIX dates back to early 2013, focusing on $p + p$ collisions at $\sqrt{s}$ = 510 GeV [56]. We will report our latest studies on J/ψ using PHENIX Run 15 $p + p$ data at $\sqrt{s} = 200$ GeV.

3. Experimental Apparatus and Data Samples

The PHENIX experiment [55] is a general-purpose detector at RHIC at Brookhaven National Laboratory for relativistic heavy-ion physics research [57]. It has broad ϕ and η acceptance coverage [58] and can collect large data samples to perform measurements at middle and forward rapidities. The tracking, particle identification, calorimeter, and muon systems of the PHENIX experiment apply various radiation detection techniques to maximize its physics capabilities.

The forward silicon tracker detector (FVTX) employs advanced silicon strip technologies and is installed as four endcaps in the forward and backward regions covering $1.2 < |\eta| < 2.2$ [59]. Its sensor contains two columns of mini-strips with 75 μm pitches in

the radial direction and lengths varying from 3.4 to 11.5 mm in the azimuthal direction. The FVTX is capable of excellent tracklet reconstruction and precise vertex determination. In addition to the FVTX, at mid-rapidity $|\eta| < 1$, the Silicon Vertex Tracker (SVX) is a four-layer barrel detector built to enhance the capabilities of the central arm spectrometers and provides excellent position resolution [60], which enables tracking at mid-rapidity.

Two muon arms are built in the forward and backward regions, far away from the beam spot, with a rapidity coverage of $1.2 < |\eta| < 2.4$ [61]. A stack of absorber/low resolution tracking layers allow for excellent muon detection and identification. Along with the three new resistive plate chambers, the rejection factor for muon from pions and kaons is in the order magnitude of 10^3. Each muon arm is equipped with a radial field magnetic spectrometer to provide precision muon tracking. The muon momentum resolution is $\delta p / p \sim 1.7\%$, allowing for an excellent performance in quarkonia reconstruction and clean separation between J/ψ and ψ' [62].

The PHENIX Electromagnetic Calorimeter (EMCAL) uses Pb as the absorber material and a shashlik design with a block size of 5.5 cm × 5.5 cm and wavelength shifting fibers to measure the electromagnetic shower energy [63]. The EMCAL can provide an excellent energy linearity and resolution for jet reconstruction.

The PHENIX experiment is also equipped with a ring image Cherenkov detector (RICH) to perform electron identification [64]. It can achieve a great electron selection performance from π, K, p separation at a very high p_T.

The beam–beam counters (BBC) are installed in both far-north and far-south directions with advanced electronics to determine the event vertex and activity [65]. BBC uses the coincidence of both sides along with a minimum ADC threshold to select MB events. The zero-degree calorimeter (ZDC) is used in an identical form for all four experiments at RHIC to characterize global event parameters in the very forward direction [66]. It can achieve the precise determination of event activity, luminosity, and forward-neutron-counting through the measurements of beam-fragment energy deposition in the far-forward direction.

With excellent detector hardware capabilities, PHENIX also designs and deploys a dedicated Level 1 trigger to collect data samples for different physics topics [67], applying high-performance computing and electronic readout technologies [68]. Many collisions occur at RHIC when the collider is running. However, only a small fraction of them are relevant to our physics studies. Thus, the MB trigger was developed for general physics studies. The MB trigger uses both BBC and ZDC to select non-diffractive dissociation processes and determine global event parameters such as the collision vertex, luminosity, and impact parameter. The overall efficiency of the MB trigger is approximately 55 ± 5%.

For charmonium physics studies, we need high statistics J/ψ samples. The dimuon trigger samples enrich J/ψ by requiring an MuID trigger to identify muons and applying quality selections to the muon tracks (MuTr). The overall efficiency of the dimuon trigger is approximately 79 ± 2%.

The PHENIX detector is also equipped with a beam clock trigger utilizing the granule timing module with fast electronics [69]. It can operate at high frequencies with an excellent timing resolution to provide precise timing information for the raw data, which allows for synchronization among subdetectors and event-building. In addition, the EMCal/RICH trigger (ERT) is dedicated to sampling hard scattering events for heavy flavor and jet physics studies.

4. Analysis

In 2015, PHENIX acquired $p + p$, $p + Al$, and $p + Au$ data with transversely polarized protons at $\sqrt{s} = 200$ GeV. Based on the PHENIX $p + p$ data, we can define the J/ψ normalized yield $R(J/\psi)$ from quantities as follows:

$$R(J/\psi) = [\frac{N_S^{J/\psi}}{N^{MB}} \frac{\epsilon_{trig}^{MB}}{\epsilon_{trig}^{J/\psi}}] \Big/ [\frac{N_S^{J/\psi}(total)}{N^{MB}(total)} \frac{\langle \epsilon_{trig}^{MB} \rangle}{\langle \epsilon_{trig}^{J/\psi} \rangle}] \times f_{coll} \quad (1)$$

The quantities are defined below:

- $N_S^{J/\psi}$: the J/ψ signal raw yield extracted from dimuon invariant mass $m_{\mu\mu}$ distribution.
- N^{MB}: the number of minimum biased events recorded.
- ϵ_{trig}^{MB}: minimum biased trigger efficiency.
- $\epsilon_{trig}^{J/\psi}$: J/ψ trigger efficiency.
- f_{coll}: correction factor for multiple collisions obtained from a data-model method.

The quantities in the bracket stand for the average value over the integral event multiplicity and the total in the parentheses means the sum over all multiplicity bins. We reconstructed J/ψ from the dimuon decay channel: $J/\psi \rightarrow \mu^+\mu^-$. It should be noted that we assumed that the luminosity, the branching ratio of $J/\psi \rightarrow \mu^+\mu^-$, the acceptance, and the reconstruction efficiency would cancel out in the normalization because they do not have significant event multiplicity dependence.

The normalized J/ψ yield $R(J/\psi)$ is plotted as a function of normalized charged particle multiplicity $N_{ch}/\langle N_{ch}\rangle$, defined as the number of tracklets reconstructed by FVTX or SVX hits. Thus, the pseudorapidity ranges of N_{ch} are $1.2 < \eta < 2.4$ for FVTX north, $-2.4 < \eta < -1.2$ for FVTX south, and $-1.0 < \eta < 1.0$ for SVX. Our results are presented in charged particle multiplicity bins of [0, 1, 2, 3, 4, 5, 6, 8, 10, 12, 19]. In our analysis, we used the MB data sample to obtain the N^{MB}. The dimuon trigger sample was used to reconstruct J/ψ. Finally, the beam clock trigger sample was used for efficiency correction and systematic uncertainties studies in a data-driven manner.

4.1. Event, Track, and J/ψ Candidate Selections

In order to achieve the best analysis results, we need to apply selections to the data samples. We applied event, track, muon, and J/ψ candidate selections to the data sample to reduce the size and ensure the quality of our analysis results. Specifically, we required the z-component of the reconstructed event vertex (z_vtx) to be within 10 cm, which was used to define the charge particle multiplicity counting.

4.2. MB Event Multiplicity Determination

We used the MB sample to determine the N^{MB}. With the N^{MB} as a function of N_{ch}, we can also obtain the $N_{MB}(total)$ by summing the distribution and $\langle N_{ch}\rangle$, taking the average on the distribution. We can then rescale the x-axis to $N_{ch}/\langle N_{ch}\rangle$ and plot the N^{MB} as a function of $N_{ch}/\langle N_{ch}\rangle$.

4.3. J/ψ Signal Extraction

After applying all selections to the dimuon sample, we were able to observe a very clear J/ψ signal with good resolution and a correct peak near the PDG value. The kinematics of the reconstructed J/ψ has $\langle p_T\rangle \sim 1.7$ GeV/c and $1.2 < |y| < 2.2$. To determine the J/ψ raw yield, we need to extract the signal in the dimuon invariant mass in data. We developed a fitting model using a single asymmetric Crystal Ball function to describe the J/ψ signal component to account for the bremsstrahlung tail and an exponential decay function to describe the background component in the data. The functional form of the signal component is given by

$$f_S(x; \alpha, n, \mu, \sigma) = \begin{cases} N\exp[-\frac{(x-\mu)^2}{2\sigma^2}], & \text{if } \left(\frac{x-\mu}{\sigma} > \alpha\right) \\ NA(B - \frac{x-\mu}{\sigma})^{-n} & \text{if } \left(\frac{x-\mu}{\sigma} \leq \alpha\right) \end{cases} \tag{2}$$

where

$$A = \left(\frac{n}{|\alpha|}\right)^n \exp\left(-\frac{|\alpha|^2}{2}\right) \tag{3}$$

and

$$B = \frac{n}{|\alpha|} - |\alpha| \tag{4}$$

The functional form of the background component is given by

$$f_B(x; D, \lambda) = De^{-\lambda x} \tag{5}$$

Hence, the total fit function is given by

$$f = N_S^{J/\psi} \cdot f_s + N_B \cdot f_B \tag{6}$$

We then used the *RooFit* package [70] to fit the data points and obtain the J/ψ signal raw yield $N_S^{J/\psi}$. The invariant mass distribution of J/ψ from the north and south muon arms for inclusive event multiplicity, along with the fits, are shown below in Figure 1.
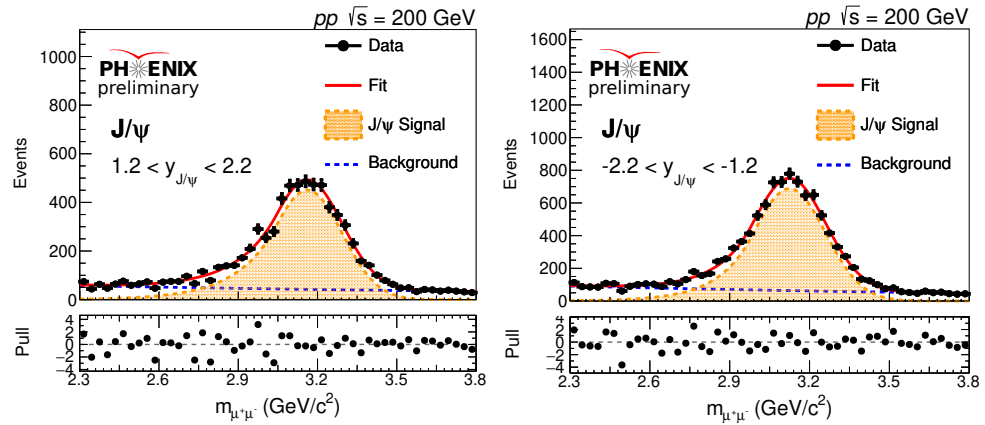

Figure 1. The dimuon invariant mass distributions of the J/ψ at $1.2 < y_{J/\psi} < 2.2$ (**left**) and $-2.2 < y_{J/\psi} < -1.2$ (**right**) with their fits are shown above. It should be noted that the south muon arm on the right has a higher J/ψ yield than the north one with the same selections because it has better performance with a higher muon efficiency in Run 2015 data collection.

The free parameters for the fits are N, A, B, μ, σ, D, and λ. We fixed A and N in the fit on the inclusive north and south muons arm samples to keep the overall shape needed to fit each $N_{ch}/\langle N_{ch} \rangle$ bin. Good statistics, with a reconstruction performance of J/ψ in the dimuon channel, can be observed in Figure 1. We sum $N_S^{J/\psi}$ of all $N_{ch}/\langle N_{ch} \rangle$ bins to obtain $N_S^{J/\psi}(total)$.

4.4. Efficiency Correction

We quoted the $\langle \epsilon_{trig}^{MB} \rangle = 55\%$ and $\langle \epsilon_{trig}^{J/\psi} \rangle = 79\%$, as mentioned in the description for the PHENIX detector. Then, we employed a data-drive method to correct the MB and J/ψ efficiencies.

To determine ϵ_{trig}^{MB} as a function of event multiplicity, we used the the RHIC beam clock trigger data. A collision is declared to have occurred if there is at least one tracklet in the FVTX or SVX. Hence, ϵ_{trig}^{MB} is the ratio of the RHIC beam clock trigger sample with BBC local level 1 trigger, which is also fired, f to the whole sample for BBC rate between 1000 and 1500 kHz. The systematic uncertainties $\sigma(\epsilon_{trig}^{MB})$ are given by the deviation of ϵ_{trig}^{MB} at a BBC rate from 600 to 800 kHz and 2000 to 2500 kHz from the nominal value 1000–1500 kHz as the upper and lower bounds, respectfully.

To determine $\epsilon_{trig}^{J/\psi}$ as a function of event multiplicity, we used the ERT trigger sample. We calculated $\epsilon_{trig}^{J/\psi}$ using the multiplicity distribution of the ERT sample with at least one track as the denominator, and the multiplicity distribution of the ERT sample with at least one track and a valid BBC vertex z-component within 200 cm as the numerator. The statistical uncertainties of the first bin $N_{ch} = 1$ are quoted as global systematic uncertainties $\sigma(\epsilon_{trig}^{J/\psi})$.

4.5. Multiple Collection Factor Correction

Multiple $p + p$ collisions may occur at RHIC. Experimentally, each collision results in a primary vertex. The number of collisions in each event generally obeys the Poisson distribution. According to our studies, the double-collision probability is at the level of a few percent.

Because we focused on J/ψ produced in a single $p + p$ collision, we needed to correct multiple collision effects in our data. We employed a data-model hybrid method to determine f_{coll}. We used a model to calculate N^{MB} as a function of N_{ch}. We divided the normalized N^{MB} distribution for the south FVTX arm near a BBC rate of 830 kHz, which consists of less than 2% of double-collisions, using the single-collision model and the ratio as f_{coll}. We quoted the deviation from the model to the PHENIX data with a BBC rate between 1000 and 1500 kHz as the systematic error on the multiple collision correction factor $\sigma(f_{coll})$, accounting for the disagreement between the model and the data.

4.6. Systematic Uncertainties Estimation

The systematic uncertainties on this measurement consist of the MB trigger efficiency, J/ψ trigger efficiency, multiple-collision correction, and J/ψ reconstruction efficiency. The J/ψ reconstruction efficiency $\epsilon_{reco}^{J/\psi}$ has a weak dependence on N_{ch}. This is treated as a constant but can be assigned using a global systematics of 5% from previous J/ψ measurements in the dimuon channel [71]. Finally, we treated individual uncertainties as uncorrelated, and thus could estimate the total systematic uncertainties as follows:

$$\sigma(total) = \sigma(\epsilon_{trig}^{MB}) \oplus \sigma(\epsilon_{trig}^{J/\psi}) \oplus \sigma(\epsilon_{reco}^{J/\psi}) \oplus \sigma(f_{coll}) \tag{7}$$

5. Results

After finishing the data analysis, we gathered all the ingredients to obtain the final results. Different underlying physics processes can be studied from different rapidity combinations of J/ψ and tracklet multiplicity measurements. Figure 2 illustrates the physics with different measurements.
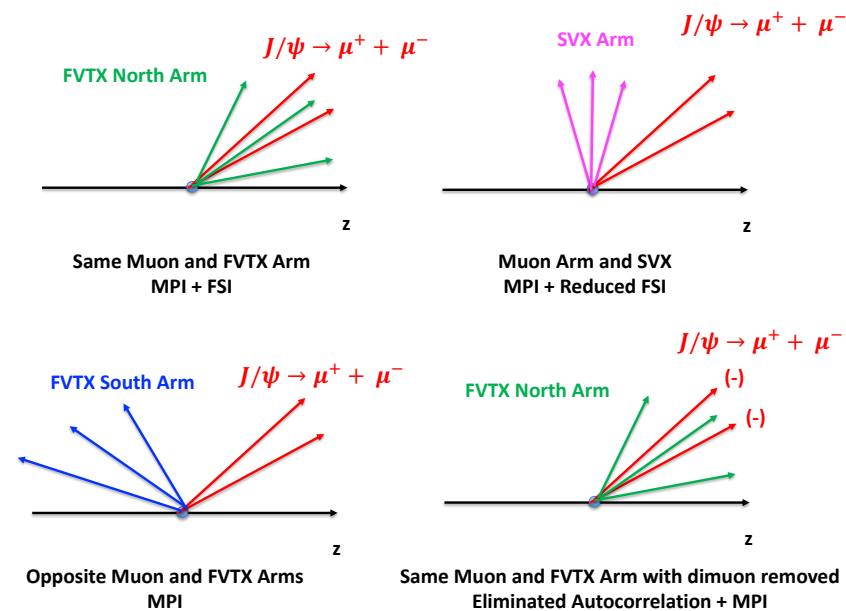

Figure 2. The definitions of four different rapidity measurements of the J/ψ with respect to the silicon tracklet measurements and the physics processes involved are illustrated above.

Phenomenologically, MPI always occurs, regardless of the rapidity of the J/ψ and the charged particles. In the PHENIX experiment, when both the J/ψ and the tracklets point in the same rapidity direction, we expect to find significant FSI contributions to

J/ψ production due to the presence of nearby particles [33]. In the elastic scenario, J/ψ kinematics will be modified. Inelastically, J/ψ may be broken up [32]. As the J/ψ moves away from the charged particles, the comover effect in the final state is expected to diminish. This can be achieved by measuring the SVX and the opposite FVTX arm for the tracklet multiplicity with respect to the muon arms. Finally, muons can also contribute to the event multiplicity. For $J/\psi \to \mu^+\mu^-$, the two muons, on average, increase the N_{ch} by approximately 1.4. After removing this autocorrelation effect from the J/ψ decayed muons, the charged particle multiplicity will become $\tilde{N}_{ch}$. We can also present the normalized J/ψ yield as a function of $\tilde{N}_{ch}/\langle\tilde{N}_{ch}\rangle$ by adjusting the x-axis in our measurement. These cases are all shown in Figure 2.

The final results of J/ψ, reconstructed from the north muon arm located in the forward-rapidity direction $1.2 < y_{J/\psi} < 2.2$ and the south muon arm located at the backward-rapidity $-2.2 < y_{J/\psi} < -1.2$ with respect to FVTX north and south and SVX measurements, are shown in Figure 3.
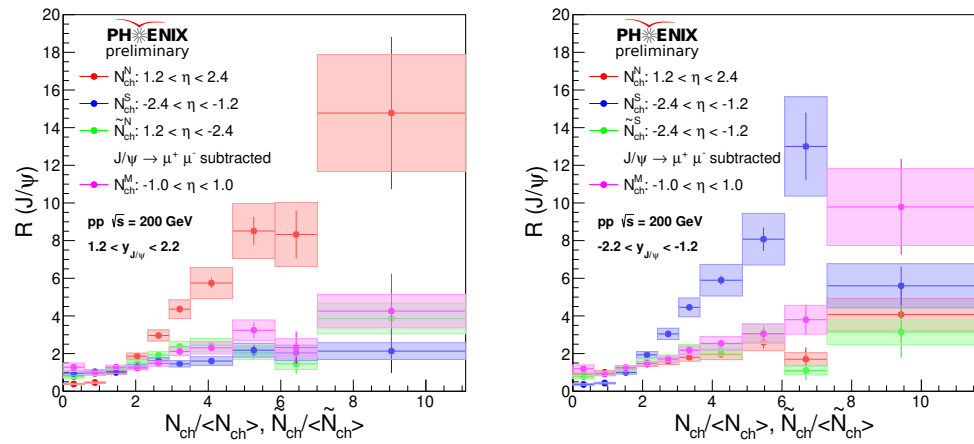

Figure 3. The J/ψ reconstructed from the north muon arm $1.2 < y_{J/\psi} < 2.2$ (**left**) and the south muon arm $-2.2 < y_{J/\psi} < -1.2$ (**right**) are shown above. The J/ψ normalized signal yields $R(J/\psi)$ from the dimuon channel are presented as a function of normalized charged particle multiplicity $N_{ch}/\langle N_{ch}\rangle$ measured by FVTX and SVX. In addition, we show the results when J/ψ and the charged particles are in the same direction, with the dimuon contribution subtracted. In terms of color convention, the FVTX north data are shown in red, FVTX south data in blue, SVX in magenta, and the dimuon-subtracted results are shown in magenta. These four sets of data points are all overlaid with each other in the same figure.

The J/ψ yields up to approximately 10 units of average charged particle multiplicity, which are measured with good precision. A stronger than linear rise is observed at the same rapidity direction between the J/ψ and the charged particles. The enhancement becomes more prominent at high-multiplicity regions. The slope decreases as the rapidity gap between the J/ψ and the charged particles increases when $N_{ch}/\langle N_{ch}\rangle > 1$. Finally, after subtracting the dimuon contributions at the same rapidity directions, the data points drop drastically and become consistent with the opposite rapidity measurements. These results imply that the FSI effect does not have a substantial impact on J/ψ production in $p+p$ collisions. However, MPI effects should be considered in order to the enhancement, particularly in the high-multiplicity region.

We also compare our data with recent measurements from STAR at RHIC [41] and ALICE at the LHC [39], as shown below.

In Figure 4, we can see that PHENIX has broader charged particle multiplicity measurements with better precision than STAR and a comparable reach to ALICE, albeit with lower precision. At a low charged-particle multiplicity, PHENIX data points are systematically below the STAR ones. In a higher-event-multiplicity region, PHENIX data points ($1.2 < |y| < 2.2$) lie in between the ALICE middle ($|y| < 0.9$) and forward-rapidity

$(2.5 < y < 4)$ measurements, filling the missing-rapidity region from ALICE. All data points have slopes significantly above 1 when $N_{ch}/\langle N_{ch}\rangle > 1$. Hence, the comparisons suggest that J/ψ produced in the middle-rapidity is generally above the forward-rapidity at both RHIC and LHC energies, which corresponds to the different phase-space regions of $x_{1,2}$ of the partons during hard interactions.
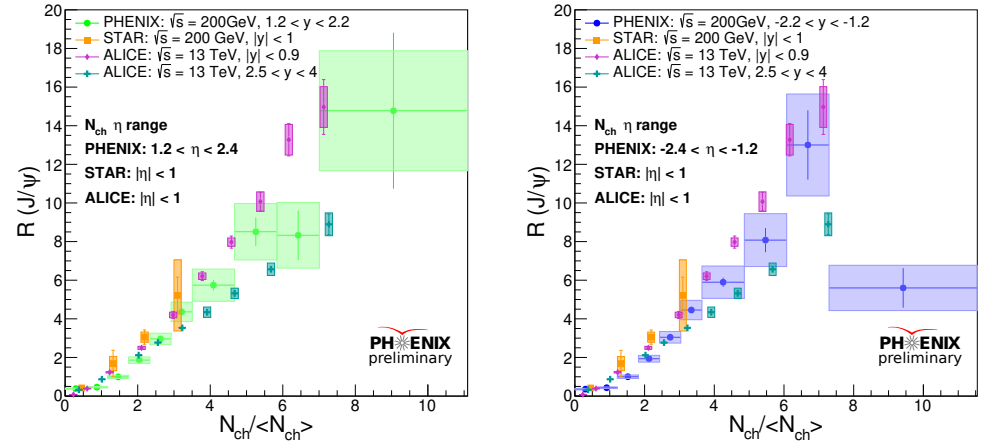

Figure 4. The J/ψ normalized yield as a function of normalized charged particle multiplicity of PHENIX, STAR [41], and ALICE [39] are all shown above. To make our results comparable with STAR and ALICE data, we present the measurements where J/ψ and tracklets are both in the north (green, **left**) and the south (blue, **right**). STAR uses the RHIC $p + p$ data at $\sqrt{s} = 200$ GeV to reconstruct J/ψ from the dielectron channel and the charged particle multiplicity, both measured at the mid-rapidity region $|y| < 1$ (orange). ALICE carries out both middle-rapidity $|y| < 0.9$ with the SPD tracklets and forward-rapidity $2.5 < y < 4$ with the V0 tracklets from $J/\psi \rightarrow e^+ e^-$ channel. All these results include daughter lepton tracks from J/ψ decay in the event multiplicity.

Finally, we compare our data with the PYTHIA 8 simulations with Monash and Detroit tunes including, and not including, the MPI effect shown in Figure 5.
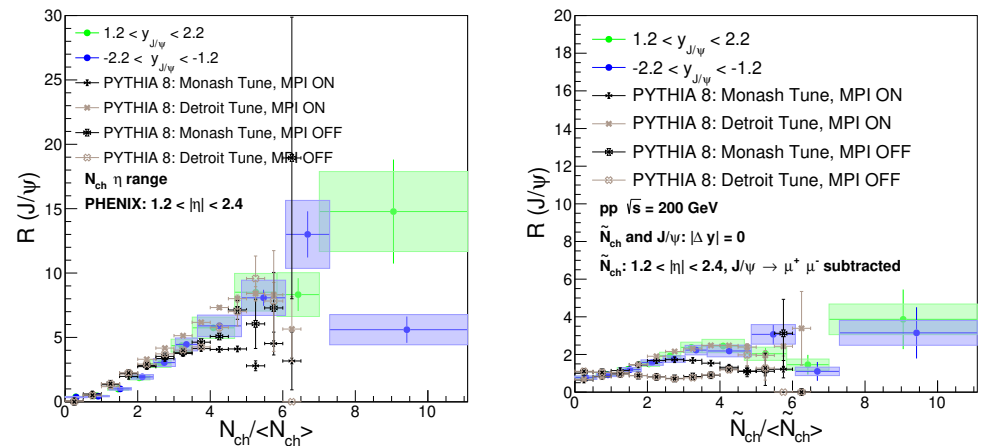

Figure 5. In the figure, the same muon arms and FVTX directions are used for J/ψ and charged particle tracklet reconstructions. J/ψ in the forward (green) and backward (blue) rapidities, and PYTHIA 8 simulations without dimuon subtraction (**left**) and with dimuon subtraction (**right**), are shown above. The PYTHIA 8 simulations present four different combinations, Monash Tune and Detroit Tune, with the MPI option turned on and off, to directly study MPI using the data.

In PYTHIA 8 $p + p$ simulations, we set up the $c\bar{c}$ event with a large $\hat{p}_T$ for J/ψ production and used general inelastic hadronic collisions to model MB events. Because it is unlikely to generate events with high multiplicities, our simulation only covers up to

$N_{ch}/\langle N_{ch}\rangle \simeq 6$ and has large statistical uncertainties at high multiplicities. Nonetheless, PYTHIA 8 simulations with different setups diverge at high multiplicities. PYTHIA 8, when using the Detroit Tune and turning on the MPI effect, can best describe the data. Hence, the MPI effect is significant for J/ψ production in $p+p$ collisions at RHIC, particularly in the high-multiplicity region.

6. Summary

We have reported the measurement of J/ψ normalized yield as a function of normal charged particle multiplicity with PHENIX Run 2015 $p+p$ collisions at $\sqrt{s}=200$ GeV. The J/ψ is reconstructed from the dimuon channel with the PHENIX muon arms in the forward rapidity. The charged particle tracklets are reconstructed with FVTX and SVX detectors. Our results are presented in different combinations of J/ψ with $\langle p_T\rangle \sim 1.7$ GeV/c and $1.2 < |y| < 2.2$ and charged particles at $1.2 < |\eta| < 2.4$ for FVTX and $|y| < 1$ for SVX up to approximately 10 units of normalized event multiplicity. The J/ψ normalized yield beyond linear scaling is observed when the J/ψ and charged particles are both measured at the same rapidity. The enhancement of J/ψ production becomes more pronounced at high event multiplicities, which could possibly be explained by MPI. The J/ψ normalized yield decreases significantly, as the rapidity gap between the J/ψ and the charged particles increases. After subtracting the dimuon contributions from the event multiplicity when the J/ψ and the charged particles point in the same rapidity direction, the results become consistent with the results where J/ψ and charged particles are produced in opposite rapidity directions, which hints at the insignificance of the final-state comover effects for J/ψ production in $p+p$ collisions.

Our forward J/ψ results lie systematically below the STAR measurement in the middle rapidity and in between the ALICE data in the forward and middle rapidities. We notice that J/ψ produced in the middle rapidity is generally below that of the forward rapidity within the same normalized charged-particle multiplicity. This allows for us to probe the parton distribution function in different phase-space regions. Finally, through the comparison of our data with PYTHIA 8 simulation using the Detroit and Monash Tunes with MPI options turned on and off, we found that the Detroit Tune with MPI on best describes our data. Hence, the MPI contribution should be included in order to precisely describe J/ψ production in $p+p$ collisions at RHIC, especially in high-multiplicity events.

To investigate the possibility of J/ψ production from jet fragmentation, we plan to look at our results in different J/ψ p_T regions. We expect J/ψ production from jets to be more likely at a high p_T. This study is currently ongoing. However, because of the limited statistics, particularly for $p_T > 3$ GeV/c, we may not achieve sufficient precision to conclude the possible J/ψ production from jet fragmentation in $p+p$ collisions at RHIC.

We are also carrying out J/ψ production in $p+Au$ collisions to test CGC calculations. In addition, the ongoing measurement of $\psi(2S)/J/\psi$ ratio in $p+p$ collisions will help us to understand charmonium hadronization. Many novel and exciting physics results regarding charmonium production in different collision systems with PHENIX data are coming in the near future.

References

1. Aubert, J.J.; Becker, U.; Biggs, P.J.; Burger, J.; Chen, M.; Everhart, G.; Goldhagen, P.; Leong, J.; McCorriston, T.; Rhoades, T.G.; et al. Experimental Observation of a Heavy Particle. *J. Phys. Rev. Lett.* **1974**, *33*, 1404–1406. [CrossRef]
2. Augustin, J.E.; Boyarski, A.M.; Breidenbach, M.; Bulos, F.; Dakin, J.T.; Feldman, G.J.; Fischer, G.E.; Fryberger, D.; Hanson, G.; Jean-Marie, B.; et al. Discovery of a Narrow Resonance in e^+e^- Annihilation. *Phys. Rev. Lett.* **1974**, *33*, 1406–1408. [CrossRef]
3. Glashow, S.L.; Iliopoulos, J.; Maiani, L. Weak Interactions with Lepton–Hadron Symmetry. *Phys. Rev. D* **1970**, *2*, 1285–1292. [CrossRef]
4. Cacciari, M.; Greco, M.; Mangano, M.L.; Petrelli, A. Charmonium Production at the Tevatron. *Phys. Lett. B* **1995**, *356*, 553–560. [CrossRef]
5. Zhao, X.; Ralf, R. Forward and midrapidity charmonium production at RHIC. *Eur. Phys. J. C* **2009**, *62*, 109–117. [CrossRef]
6. Stahl, A.G. Charmonium production in pp, pPb and PbPb collisions with CMS. *J. Phys. Conf. Ser.* **2017**, *832*, 012031. [CrossRef]
7. Collins, J.C.; Soper, D.E.; Sterman, G. Factorization of Hard Processes in QCD. *Adv. Ser. Direct. High Energy Phys.* **1989**, *5*, 1–91.
8. Wong, C.Y. *Introduction to High-Energy Heavy-Ion Collisions*; World Scientific: Singapore, 1994; 516p.
9. Feynman, R.P. The behavior of hadron collisions at extreme energies. *Conf. Proc. C* **1969**, *33*, 237–258.
10. Soper, D.E. Parton distribution functions. *Nucl. Phys. B Proc. Suppl.* **1997**, *53*, 69–80. [CrossRef]
11. Dias de Deus, J.; Pajares, C. String Percolation and the Glasma. *Phys. Lett. B* **2011**, *695*, 211–213. [CrossRef]
12. Armesto, N.; Braun, M.A.; Ferreiro, E.G.; Pajares, C. Percolation Approach to Quark-Gluon Plasma and J/ψ Suppression. *Phys. Rev. Lett.* **1996**, *77*, 3736 [CrossRef]
13. Gelis, F.; Iancu, E.; Jalilian-Marian, J.; Venugopalan, R. The Color Glass Condensate. *Annu. Rev. Nucl. Part. Sci.* **2010**, *60*, 463–489. [CrossRef]
14. Ma, Y.-Q.; Venugopalan, R. Comprehensive Description of J/ψ Production in Proton-Proton Collisions at Collider Energies. *Phys. Rev. Lett.* **2013**, *113*, 192301. [CrossRef]
15. Braun, M.A.; Del Moral, F.; Pajares, C. Percolation of strings and the first RHIC data on multiplicity and transverse momentum distributions. *Phys. Rev. C* **2002**, *65*, 024907. [CrossRef]
16. Shao, H.S. Initial state radiation effects in inclusive J/ψ production at B factories. *J. High Energ. Phys.* **2014**, *2014*, 182. [CrossRef]
17. Buonocore, L.; Nason, P.; Tramontano, F. Heavy quark radiation in NLO+PS POWHEG generators. *Eur. Phys. J. C* **2018**, *78*, 151. [CrossRef]
18. Catani, S.; Grazzini, M.; Torre, A. Transverse-momentum resummation for heavy-quark hadroproduction. *Nucl. Phys. B* **2014**, *890*, 518–538 [CrossRef]
19. Berger, E.L.; Meng, R. Transverse momentum distributions for heavy quark pairs. *Phys. Rev. D* **1994**, *49*, 3248–3260. [CrossRef] [PubMed]
20. Anastasiou, C.; Dixon, L.; Melnikov, K.; Petriello, F. High precision QCD at hadron colliders: Electroweak gauge boson rapidity distributions at NNLO. *Phys. Rev. D* **2004**, *69*, 094008 [CrossRef]
21. Blok, B.; Dokshitzer, Y.; Frankfurt, L.; Strikman, M. pQCD physics of multiparton interactions. *Eur. Phys. J. C* **2012**, *72*, 1963. [CrossRef]
22. Bartalini, P.; Berger, E.L.; Blok, B.; Calucci, G.; Corke, R.; Diehl, M.; Dokshitzer, Y.; Fano, L.; Frankfurt, L.; Gaunt, J.R.; et al. Multi-Parton Interactions at the LHC. *arXiv* **2011**, arXiv:1111.0469.
23. Soto, J. Overview of Non-Relativistic QCD. *Eur. Phys. J. A* **2007**, *31*, 705–710. [CrossRef]
24. Berger, E.L.; Jones, D. Inelastic photoproduction of J/ψ and Y by gluons. *Phys. Rev. D* **1981**, *23*, 1521. [CrossRef]
25. Bain, R.; Dai, L.; Hornig, A.; Leibovich, A.K.; Makris, Y.; Mehen, T. Analytic and Monte Carlo Studies of Jets with Heavy Mesons and Quarkonia. *JHEP* **2016**, *6*, 121 [CrossRef]
26. Cho, P.L.; Leibovich, A.K. Color octet quarkonia production. *Phys. Rev. D* **1996**, *53*, 150–162. [CrossRef] [PubMed]
27. Adare, A. et al. [PHENIX Collaboration]. Transverse momentum dependence of J/ψ polarization at midrapidity in $p+p$ collisions at $\sqrt{s} = 200$ GeV. *Phys. Rev. D* **2010**, *82*, 012001 [CrossRef]
28. Ma, Y.-Q.; Vogt, R. Quarkonium production in an improved color evaporation model. *Phys. Rev. D* **2016**, *94*, 114029. [CrossRef]
29. Andronic, A.; Braun-Munzinger, P.; Köhler, M.K.; Redlich, K.; Stachel, J. Transverse momentum distributions of charmonium states with the statistical hadronization model. *Phys. Lett. B* **2019**, *797*, 134836 [CrossRef]
30. Kotko, P.; Motyka, L.; Stasto, A. Color Reconnection Effects in J/ψ Hadroproduction. *arXiv* **2023**, arXiv:2303.13128.
31. Crkovska, J. Study of the J/ψ Production in pp Collisions at $\sqrt{s_{NN}} = 5.02$ TeV and of the J/ψ Production Multiplicity Dependence in p-Pb Collisions at $\sqrt{s_{NN}} = 8.16$ TeV with ALICE at the LHC. High Energy Physics-Experiment. Ph.D. Thesis, Université Paris-Saclay, Paris, France, 2018.
32. Bahmani, M.; Kikoła, D.; Kosarzewski, L. A technique to study the elastic and inelastic interaction of quarkonium with hadrons using femtoscopic correlations. *Eur. Phys. J. C* **2021**, *81*, 305. [CrossRef]
33. Werner, K.; Guiot, B.; Karpenko, I.; Pierog, T. Analysing radial flow features in p–Pb and pp collisions at several TeV by studying identified particle production in EPOS3. *Phys. Rev. C* **2014**, *89*, 064903. [CrossRef]
34. Bailung, Y. Measurement of D-meson production as a function of charged-particle multiplicity in proton–proton collisions at $\sqrt{s} = 13$ TeV with ALICE at the LHC. *PoS LHCP* **2021**, *2021*, 190.
35. Weber, S.G.; Dubla, A.; Andronic, A.; Morsch, A. Elucidating the multiplicity dependence of J/ψ production in proton–proton collisions with PYTHIA8. *Eur. Phys. J. C* **2019**, *79*, 36. [CrossRef]

36. Norrbin, E.; Sjöstrand, T. Production mechanisms of charm hadrons in the string model. *Phys. Lett. B* **1998**, *442*, 407–416. [CrossRef]
37. Acharya, S. et al. [ALICE Collaboration]. Inclusive J/ψ production at mid-rapidity in pp collisions at $\sqrt{s}$ = 5.02 TeV. *JHEP* **2019**, *10*, 84.
38. Abelev, B. et al. [ALICE Collaboration]. J/ψ polarization in pp collisions at $\sqrt{s}$ = 7 TeV. *Phys. Rev. Lett.* **2012**, *108*, 082001. [CrossRef]
39. Acharya, S. et al. [ALICE Collaboration]. Multiplicity dependence of J/ψ production at midrapidity in pp collisions at $\sqrt{s}$ = 13 TeV. *Phys. Lett. B* **2020**, *810*, 135758. [CrossRef]
40. Acharya, S. et al. [ALICE Collaboration]. Forward rapidity J/ψ production as a function of charged-particle multiplicity in pp collisions at $\sqrt{s}$ = 5.02 and 13 TeV. *JHEP* **2022**, *6*, 15
41. Adam, J. et al. [STAR Collaboration]. J/ψ production cross section and its dependence on charged-particle multiplicity in $p + p$ collisions at $\sqrt{s}$ = 200 GeV. *Phys. Lett. B* **2018**, *786*, 87–93. [CrossRef]
42. Thakur, D.; De, S.; Sahoo, R.; Dansana, S. Role of multiparton interactions on J/ψ production in $p + p$ collisions at LHC energies. *Phys. Rev. D* **2018**, *97*, 094002. [CrossRef]
43. Egede, U.; Hadavizadeh, T.; Singla, M.; Skands, P.; Vesterinen, M. The role of multi-parton interactions in doubly-heavy hadron production. *Eur. Phys. J. C* **2022**, *82*, 773. [CrossRef]
44. Gotsman, E.; Levin, E. High energy QCD: Multiplicity dependence of quarkonia production. *Eur. Phys. J. C* **2021**, *81*, 99. [CrossRef]
45. Sjöstr, T.; Ask, S.; Christiansen, J.R.; Corke, R.; Desai, N.; Ilten, P.; Mrenna, S.; Prestel, S.; Rasmussen, C.O.; Skands, P.Z. An Introduction to PYTHIA 8.2. *Comput. Phys. Commun.* **2015**, *191*, 159–177. [CrossRef]
46. Aguilar, M.R.; Chang, Z.; Elayavalli, R.K.; Fatemi, R.; He, Y.; Ji, Y.; Kalinkin, D.; Kelsey, M.; Mooney, I.; Verkest, V. PYTHIA 8 underlying event tune For RHIC energies. *Phys. Rev. D* **2022**, *105*, 016011. [CrossRef]
47. Skands, P.; Carrazza, S.; Rojo, J. Tuning PYTHIA 8.1: The Monash 2013 Tune. *Eur. Phys. J. C* **2014**, *74*, 3024. [CrossRef]
48. Butenschoen, M.; Kniehl, B.A. J/ψ polarization at Tevatron and LHC: Nonrelativistic-QCD factorization at the crossroads. *Phys. Rev. Lett.* **2012**, *108*, 172002 [CrossRef] [PubMed]
49. Canelli, F. et al. [CMS Collaboration]. Study of J/ψ production inside jets in pp collisions at $\sqrt{s}$ = 8 TeV. *Phys. Lett. B* **2020**, *804*, 135409. [CrossRef]
50. Bruno, G. et al. [CMS Collaboration]. Fragmentation of jets containing a prompt J/ψ meson in *PbPb* and *pp* collisions at $\sqrt{s_{NN}}$ = 5.02 TeV. *Phys. Lett. B* **2022**, *825*, 136842. [CrossRef]
51. Aaij, R. et al. [LHCb Collaboration]. Study of J/ψ Production in Jets. *Phys. Rev. Lett.* **2017**, *118*, 192001. [CrossRef]
52. Yuan, F.; Chao, K.-T. Diffractive J/ψ production as a probe of the gluon component in the Pomeron. *Phys. Rev. D* **1998**, *57*, 5658–5662. [CrossRef]
53. Sahoo, R. et al. [ALICE Collaboration]. Measurement of inelastic, single- and double-diffraction cross sections in proton–proton collisions at the LHC with ALICE. *Eur. Phys. J. C* **2013**, *73*, 2456 [CrossRef] [PubMed]
54. Aad, G. et al. [ATLAS Collaboration]. Measurement of differential cross sections for single diffractive dissociation in $\sqrt{s}$ = 8 TeV *pp* collisions using the ATLAS ALFA spectrometer. *JHEP* **2020**, *10*, 182.
55. Adcox, K. et al. [PHENIX Collaboration]. PHENIX detector overview. *Nucl. Instrum. Methods Phys. Res. Sec. A* **2003**, *499*, 469. [CrossRef]
56. Adare, A. et al. [PHENIX Collaboration]. Measurements of double-helicity asymmetries in inclusive J/ψ production in longitudinally polarized $p + p$ collisions at $\sqrt{s}$ = 510 GeV. *Phys. Rev. D* **2016**, *94*, 112008 [CrossRef]
57. Adcox, K. et al. [PHENIX Collaboration]. Formation of dense partonic matter in relativistic nucleus–nucleus collisions at RHIC: Experimental evaluation by the PHENIX Collaboration. *Nucl. Phys. A* **2005**, *757*, 184–283 [CrossRef]
58. Brooks, M.L. Physics Potential of and Status Report on the PHENIX Experiment. In Proceedings of the ICPAQGP, Jaipur, India, 17–21 March 1997; pp. 326–334
59. Aidala, C. et al. [PHENIX Collaboration]. The PHENIX Forward Silicon Vertex Detector. *Nucl. Instrum. Meth. A* **2014**, *755*, 44–61. [CrossRef]
60. Akiba, Y. Proposal for a Silicon Vertex Tracker (VTX) for the PHENIX Experiment. DOE Contact Number DE-AC02-98CH10886, United States: N. p. 2004. Available online: https://www.bnl.gov/isd/documents/28627.pdf (accessed on 30 May 2023).
61. Akikawa, H. et al. [PHENIX Collaboration]. PHENIX Muon Arms. *Nucl. Instrum. Meth. A* **2003**, *499*, 537–548. [CrossRef]
62. Newby, J. Single and Dimuon Reconstruction Performance of the PHENIX South Muon Arm. Poster for Quark Matter 2002. Available online: https://www.phenix.bnl.gov/WWW/publish/rjnewby/QM2002Poster.pdf (accessed on 28 May 2023).
63. Aphecetche, L. et al. [PHENIX Collaboration]. PHENIX calorimeter. *Nucl. Instrum. Meth. A* **2003**, *499*, 521–536. [CrossRef]
64. Akiba, Y. Ring imaging Cherenkov detector of PHENIX experiment at RHIC. *Nucl. Instrum. Meth. A* **1999**, *433*, 143–148. [CrossRef]
65. Allen, M. et al. [PHENIX Collaboration]. PHENIX inner detectors. *Nucl. Instrum. Meth. A* **2003**, *499*, 549–559. [CrossRef]
66. Adler, C.; Denisov, A.; Garcia, E.; Murray, M.; Stroebele, H.; White, S. The RHIC zero degree calorimeter. *Nucl. Instrum. Meth. A* **2001**, *470*, 6499. [CrossRef]
67. Belikov, S.; Hill, J.; Lajoie, J.; Skank, H.; Sleege, G. PHENIX trigger system. *Nucl. Instrum. Meth. A* **2002**, *494*, 541–547. [CrossRef]
68. Lajoie, J.G.; Woh, F.K.; Hill, J.C.; Petridis, A.; Wood, L.; Cook, K.; Plagge, T.; Skank, H.D.; Thomas, W.D.; Sleege, G.A. The PHENIX Level-1 trigger system. In Proceedings of the 999 IEEE Conference on Real-Time Computer Applications in Nuclear Particle and Plasma Physics. 11th IEEE NPSS Real Time Conference. Conference Record (Cat. No.99EX295), Santa Fe, NM, USA, 14–18 June 1999; p. 517.

69.   Adler, S.S.; Allen, M.; Alley, G.; Amirikas, R.; Arai, Y.; Awes, T.C.; Barish, K.N.; Barta, F.; Batsouli, S.; Belikov, S.; et al. PHENIX on-line systems. *Nucl. Instrum. Meth. A* **2003**, *499*, 560–592. [CrossRef]
70.   Verkerke, W.; Kirkby, D. The RooFit toolkit for data modeling. In *Statistical Problems in Particle Physics, Astrophysics and Cosmology*; Imperial College Press: Oxford, UK, 2006; pp. 186–189.
71.   Acharya, U.A. et al. [PHENIX Collaboration]. J/ψ and $\psi(2S)$ production at forward rapidity in $p + p$ collisions at $\sqrt{s} = 510$ GeV. *Phys. Rev. D* **2020**, *101*, 052006. [CrossRef]